













A 3 Gyr White Dwarf with Warm Dust Discovered via the Backyard Worlds: Planet 9 Citizen Science Project

John H. Debes¹ , Melina Thévenot², Marc J. Kuchner³ , Adam J. Burgasser⁴ , Adam C. Schneider⁵ , Aaron M. Meisner^{6,13} ,
Jonathan Gagné⁷ , Jacqueline K. Faherty⁸ , Jon M. Rees⁴, Michaela Allen², Dan Caselden², Michael Cushing⁹ ,
John Wisniewski¹⁰ , Katelyn Allers¹¹ 
The Backyard Worlds: Planet 9 Collaboration²
and
The Disk Detective Collaboration¹²

¹ Space Telescope Science Institute, 3700 San Martin Drive, Baltimore, MD 21218, USA; debes@stsci.edu

² Backyard Worlds: Planet 9, USA

³ NASA Goddard Space Flight Center, Exoplanets and Stellar Astrophysics Laboratory, Code 667, Greenbelt, MD 20771, USA

⁴ Department of Physics, Center for Astrophysics and Space Sciences, Mail Code 0424, 9500 Gilman Drive, La Jolla, CA 92093-0424, USA

⁵ School of Earth and Space Exploration, Arizona State University, Tempe, AZ 85282, USA

⁶ National Optical Astronomy Observatory, 950 North Cherry Avenue, Tucson, AZ 85719, USA

⁷ Institute for Research on Exoplanets, Université de Montréal, 2900 Boulevard Édouard-Montpetit, Montréal QC H3T 1J4, Canada

⁸ Department of Astrophysics, American Museum of Natural History, Central Park West at 79th Street, New York, NY 10024, USA

⁹ Department of Physics and Astronomy, University of Toledo, Toledo, OH 43606, USA

¹⁰ Homer L. Dodge Department of Physics and Astronomy, The University of Oklahoma, 440 West Brooks Street, Norman, OK 73019, USA

¹¹ Physics and Astronomy Department, Bucknell University, 701 Moore Avenue, Lewisburg, PA 17837 Norman, OK 73019, USA

¹² Disk Detective, USA

Received 2018 November 30; revised 2019 January 29; accepted 2019 February 1; published 2019 February 19

Abstract

Infrared excesses due to dusty disks have been observed orbiting white dwarfs with effective temperatures between 7200 and 25,000 K, suggesting that the rate of tidal disruption of minor bodies massive enough to create a coherent disk declines sharply beyond 1 Gyr after white dwarf formation. We report the discovery that the candidate white dwarf LSPM J0207+3331, via the Backyard Worlds: Planet 9 citizen science project and Keck Observatory follow-up spectroscopy, is hydrogen dominated with a luminous compact disk ($L_{\text{IR}}/L_{\star} = 14\%$) and an effective temperature nearly 1000 K cooler than any known white dwarf with an infrared excess. The discovery of this object places the latest time for large-scale tidal disruption events to occur at ~ 3 Gyr past the formation of the host white dwarf, making new demands of dynamical models for planetesimal perturbation and disruption around post-main-sequence planetary systems. Curiously, the mid-infrared photometry of the disk cannot be fully explained by a geometrically thin, optically thick dust disk as seen for other dusty white dwarfs, but requires a second ring of dust near the white dwarf's Roche radius. In the process of confirming this discovery, we found that careful measurements of *WISE* source positions can reveal when infrared excesses for white dwarfs are co-moving with their hosts, helping distinguish them from confusion noise.

Key words: circumstellar matter – planetary systems – stars: individual (LSPM J0207+3331) – white dwarfs

1. Introduction

White dwarfs with infrared (IR) excesses hold critical clues to the long-term evolution and chemistry of minor bodies in orbit around stars outside the solar system. About 1%–4% of white dwarfs have detectable IR excesses due to geometrically flat and optically thick dust disks (von Hippel et al. 2007; Debes et al. 2011; Barber et al. 2014; Bonsor et al. 2017). These disks are believed to be caused by the tidal disruption of rocky bodies that then accrete onto the surface of the host white dwarf (Debes & Sigurdsson 2002; Jura 2003). Because white dwarfs are sensitive probes to the accretion of material, the atomic abundance of the dust is revealed through spectroscopy of the white dwarf photosphere (Zuckerman et al. 2007). Nearly 25%–50% of white dwarfs show dust accretion, implying that most white dwarfs have some flux of rocky bodies entering within their tidal disruption radius over their cooling lifetime (Koester et al. 2014; Hollands et al. 2018). While very old white dwarfs show photospheric evidence of

dust accretion, dusty IR excesses have previously only been seen around white dwarfs with $T_{\text{eff}} > 7000$ K or a cooling age of ~ 1 Gyr (Farihi et al. 2008; Barber et al. 2014).

We report the discovery that the high proper motion object and candidate white dwarf, LSPM J0207+3331, has a hydrogen-dominated atmosphere with an IR excess. Lépine & Shara (2005) first identified LSPM J0207+3331 as a high proper motion object, and Gentile Fusillo et al. (2019) identified it as a candidate white dwarf (WD J020733.81+333129.53) with $T_{\text{eff}} = 5790$ and $\log g = 8.06$ if it had a hydrogen-dominated atmosphere. We show through the construction of a multi-wavelength spectral energy distribution (SED) that it possesses a $L_{\text{IR}}/L_{\star} \sim 0.14$ and hosts a strong IR excess with $L_{\text{IR}}/L_{\star} \sim 0.13$, consistent with a significant amount of dust filling the region interior to the Roche disruption radius of the white dwarf.

The independent identification that this object was a white dwarf and the discovery of the IR excess were made by citizen scientists of the Backyard Worlds: Planet 9 citizen science project. This project is primarily designed to discover high

¹³ Hubble Fellow.

Table 1
Photometry and Astrometry of LSPM J0207+3331

Band	Mag.
<i>GALEX</i> NUV	21.92 ± 0.62
<i>G</i> _{BP}	17.87 ± 0.01
<i>g</i>	17.86 ± 0.02
<i>G</i>	17.52 ± 0.01
<i>r</i>	17.49 ± 0.02
<i>G</i> _{RP}	17.03 ± 0.01
<i>i</i>	17.34 ± 0.02
<i>z</i>	17.34 ± 0.02
<i>J</i> _{2MASS}	16.6 ± 0.1
<i>H</i> _{2MASS}	16.3 ± 0.2
<i>K</i> _{s,2MASS}	15.9 ± 0.3
<i>W1</i>	15.08 ± 0.03
<i>W2</i>	14.20 ± 0.03
<i>W3</i>	12.2 ± 0.3
<i>Gaia</i> Second Data Release (DR2) ID	325899163483416704
<i>Gaia</i> DR2 Parallax	22.44 ± 0.20 mas
<i>Gaia</i> DR2 $\mu_{\alpha} \cos(\delta)$	170.0 ± 0.3 mas
<i>Gaia</i> DR2 μ_{δ}	-25.4 ± 0.3 mas

proper motion *WISE* sources, with a focus on finding nearby brown dwarfs and new planets in the outer solar system (Kuchner et al. 2017). The project’s volunteers identify high proper motion sources by viewing flipbooks of four different epochs of unsmoothed *WISE* images (Meisner et al. 2018) at a Zooniverse website (www.backyardworlds.org). They have also developed their own online tools for interrogating the *WISE* data (Caselden et al. 2018).

In Section 2 we discuss the discovery and confirmation of LSPM J0207+3331 as a nearby white dwarf with an IR excess. In Section 3 we derive the parameters for the host star and its dusty disk, and finally in Section 4 we discuss the significance of this discovery in the context of previously known dusty white dwarfs.

2. Discovery and Confirmation of an Infrared Excess around LSPM J0207+3331

LSPM J0207+3331 was first flagged as an interesting candidate white dwarf by the Backyard Worlds: Planet 9 citizen scientist Melina Thévenot, who alerted the science team of its coordinates and its unusually red AllWISE *W1*–*W2* color for a white dwarf: $W1-W2 = 0.92 \pm 0.05$, which is indicative of a significant IR excess consistent with a dusty disk (Hoard et al. 2013). Its AllWISE photometry is free from artifacts or obvious contaminants, with no significant variability in the Level 1b epoch data for either the *WISE* or NEOWISE photometry (Wright et al. 2010). Both photometry taken in 2010/2011 during *WISE*’s main mission and over the 3.5 years of NEOWISE epochs were consistent within the uncertainties, and thus we average the *W1*/*W2* magnitudes between the missions (Mainzer et al. 2011, 2014). We also obtained *GALEX* near-ultraviolet (NUV) photometry (Bianchi et al. 2014), *g*, *r*, *i*, *z* photometry from the Pan-STARRS PS1 catalog (Chambers et al. 2016), and near-IR photometry from 2MASS (Skrutskie et al. 2006). A table of all photometry obtained is listed in Table 1.

In addition to photometry, we obtained medium-resolution near-IR spectra of LSPMJ0207+3331 using the Near-Infrared

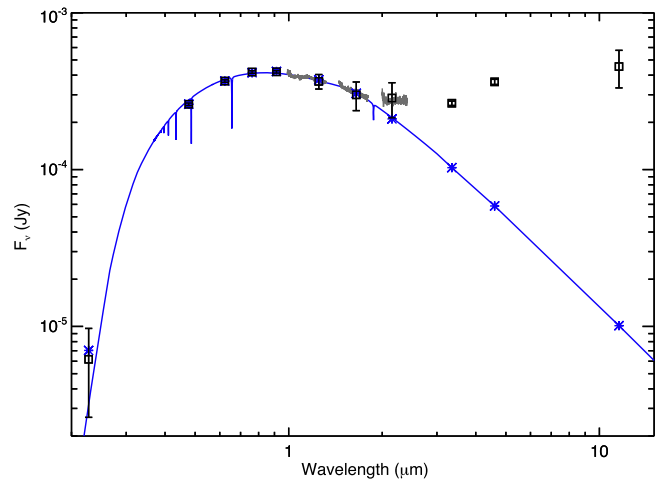


Figure 1. SED of the LSPM J0207+3331 system. Black squares represent *GALEX* NUV, Pan-STARRS *griz*, 2MASS, and AllWISE photometry. The gray lines represent the NIRES spectra. Overplotted are the predicted flux densities from our best-fit white dwarf photometric model, and a comparable model from a publicly available grid of DA spectra (Tremblay & Bergeron 2009; Koester 2010).

Echelle Spectrometer (NIREs) on the Keck II telescope (Wilson et al. 2004). The data were obtained on 2018 October 27 in partly cloudy conditions. NIREs has a fixed configuration, and covers a wavelength range of 0.94–2.45 μm at a resolution of ~ 2700 , using a slit width of $0''.55$. We obtained 12 exposures of 300 s each, nodding $5''$ along the slit between exposures for sky subtraction (3 complete ABBA sequences), at a mean airmass of 1.14 and with the slit aligned at the parallactic angle. We also obtained spectra for HD 13869, an A0V star with $V_{\text{mag}} = 5.249$, at a similar airmass for telluric correction and flux calibration. Dark and flat field frames were obtained at the end of the night. The data were reduced using a modified version of Spextool (Cushing et al. 2004), following the standard procedure. Wavelength calibration was determined using telluric lines, with a resulting rms scatter of 0.073 \AA . The spectra for each A–B pair were extracted individually and then combined together with the other extracted pairs. The telluric correction procedure was carried out as detailed in Vacca et al. (2003).

The final SED of the system is shown in Figure 1 compared to a best-fit model of the white dwarf as discussed in Section 3. As can be seen, a clear excess occurs just longward of the *H* band, confirmed both by the NIREs spectrum and the lower signal-to-noise ratio (S/N) 2MASS photometry. The excess increases beyond $5 \mu\text{m}$ with a low S/N detection of LSPM J0207+3331 in *W3*, implying significant amounts of colder dust in the system. The inferred flux density at $12 \mu\text{m}$ is comparable to the peak flux density of the white dwarf.

The *Gaia* photometry and parallax of the system also implies that LSPM J0207+3331 is a cool white dwarf (Gaia Collaboration et al. 2018). The parallax, 22.44 ± 0.20 mas, implies a distance of 44.6 ± 0.4 pc assuming a linear propagation of the parallax uncertainty. Based on *Gaia* photometry+parallax alone, LSPM J0207+3331 is consistent with a mass of $0.62 M_{\odot}$ and a cooling age of ~ 3 Gyr (Gentile Fusillo et al. 2019).

Following the initial recognition of its large proper motion in Backyard Worlds, we determined its *WISE* proper motion for *WISE*-only detections of LSPM J0207+3331 via a Monte Carlo fitting (Theissen et al. 2017) of the individual epoch positions,

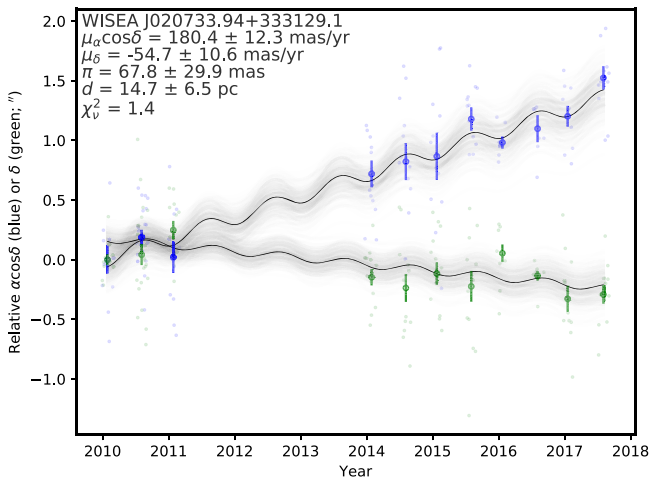


Figure 2. Proper motion fits to *WISE* and *NEOWISE* images of LSPM J0207+3331, with blue symbols corresponding to proper motion in R.A. and green symbols corresponding to proper motion in decl. Our fits to the existing *WISE* detections of the white dwarf show that the mid-IR source has common proper motion to the *Gaia* visible detection. This common proper motion, which is consistent within the uncertainties, provides a direct confirmation that the infrared excess measured is co-located with the white dwarf and not background contamination. A parallax is not significantly detected with the *WISE* epochs alone.

resulting in $\mu_{\alpha} \cos(\delta) = 180 \pm 12$ mas and $\mu_{\delta} = -55 \pm 11$ mas (Figure 2). This is consistent within the uncertainties to the reported proper motion ($\mu_{\alpha} \cos(\delta) = 170.0 \pm 0.3$ mas and $\mu_{\delta} = -25.4 \pm 0.3$ mas) of the object in the *Gaia* DR2 catalog (Gaia Collaboration et al. 2018) and the LSPM catalog (Lépine & Shara 2005).

The combination of a common proper motion to the *WISE* mid-IR source and the presence of IR excess in the NIRES spectrum (with maximum angular extent of $1''.5$), confirms that the excess is physically associated with LSPM J0207+3331 and located <67 au from the star.

3. Determining the Origin of the IR Excess

Before modeling the IR excess, we used existing observations to constrain the atmospheric composition, effective temperature (T_{eff}), and gravity of LSPM J0207+3331. Figure 3 shows a weak detection of the hydrogen Paschen β line at $1.28 \mu\text{m}$ in the NIRES spectrum, making LSPM J0207+3331 a DA white dwarf. We then fit the NUV, visible, and *J* photometry to DA white dwarf cooling models¹⁴ to infer the white dwarf properties (Holberg & Bergeron 2006; Kowalski & Saumon 2006; Bergeron et al. 2011; Tremblay et al. 2011). To obtain a best fit, we minimized a χ^2 metric over our grid of models using the reported *Gaia* parallax. We estimated statistical uncertainties within a 95% confidence interval. The best-fit $T_{\text{eff}} = 6120_{-57}^{+48}$ K, while the best-fit gravity is 8.16 ± 0.03 . Based on the cooling models we used, this implies $M = 0.69_{-0.02}^{+0.01} M_{\odot}$ and a cooling age of 3 ± 0.2 Gyr. Based on the best-fit temperature, mass, and gravity, we infer a radius of $0.011 R_{\odot}$, and a bolometric luminosity of $1.6 \times 10^{-4} L_{\odot}$. Our temperature and gravity determinations are similar to those reported by Gentile Fusillo et al. (2019), although they report a lower temperature ($T_{\text{eff}} = 5790 \pm 110$ K) and lower gravity (8.06 ± 0.07) than what we find using the Pan-STARRS photometry.

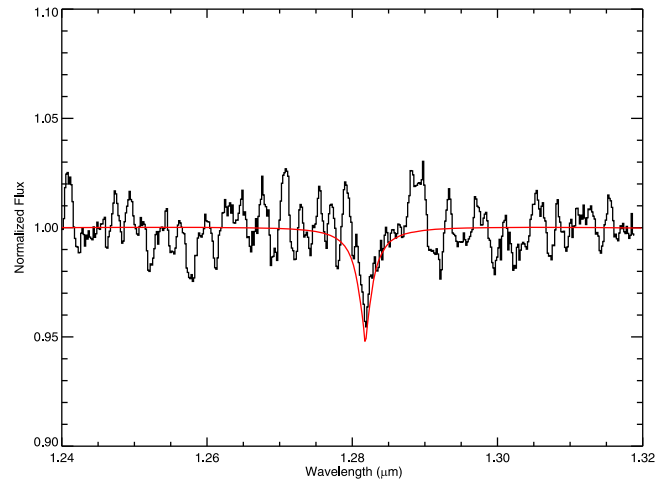


Figure 3. A 7 pixel boxcar smoothed NIRES spectrum of LSPM J0207+3331 around the Pa- β absorption line. The red line is an interpolated model from publicly available cubically interpolated DA synthetic spectra (Tremblay & Bergeron 2009; Koester 2010) with $T_{\text{eff}} = 6120$ K and $\log g = 8.16$. The line depth provides strong evidence that the white dwarf is a DA and is not suffering from any interstellar extinction that might produce a spuriously low T_{eff} .

We first attempted to explain the excess as due to a cool dwarf companion. We compared the near-IR spectrum to a series of binary models. We combined our spectral white dwarf models with companion spectra with temperatures ranging from 800 to 3500 K, drawn from the BT Settl models (Allard et al. 2012). We assumed $\log g = 5.0$ below $T_{\text{eff}} = 1200$ K and $\log g = 5.5$ above. The secondary spectra were scaled to minimize the χ^2 difference between observed and binary model spectra, and corresponding radii determined from this scale factor. For the lowest-temperature models (e.g., T dwarfs), the corresponding radii were vanishingly small ($<0.01 R_{\odot}$) as strong molecular features would otherwise contaminate the smooth continuum shape seen with NIRES. For the highest-temperature models (e.g., M dwarfs), radii were similarly small due to the higher surface fluxes. The best-fit model was for a $T_{\text{eff}} = 1600$ K secondary, and while this was significantly better than a bare white dwarf photosphere, it still required a secondary radius ($0.036 R_{\odot}$) well below that predicted by evolutionary models ($0.08 R_{\odot}$ Burrows et al. 2001; Baraffe et al. 2003). The left panel of Figure 4 compares the best-fit secondary radii to evolutionary model predictions for 1, 3 and 5 Gyr; in all cases, the inferred radii are far below that expected for a hydrogen electron-degenerate object, ruling out the possibility that the excess arises from a companion.

We next attempted to fit the observed IR excess with a face-on optically thick disk that fills the available orbital space as is traditional for most white dwarf disk modeling (Jura 2003; Rocchetto et al. 2015; Denny et al. 2017). For LSPM J0207+3331, this implies a maximum L_{IR}/L_{*} of ~ 0.13 , assuming an inner disk temperature of 1800 K and an outer radius consistent with a Roche disruption radius of $0.69 R_{\odot}$. This model failed to fit the observed data, overproducing flux between the near-IR and W1 and underpredicting the observed flux at W2 and W3. Adjusting either the inner radius of the disk or the inclination forced a decent fit to the short wavelength data, but still failed to explain the fairly bright observed mid-IR flux beyond $4 \mu\text{m}$. Similarly, increasing the outer radius of the disk to be consistent with a larger Roche radius, as would be assumed

¹⁴ <http://www.astro.umontreal.ca/~bergeron/CoolingModels/>

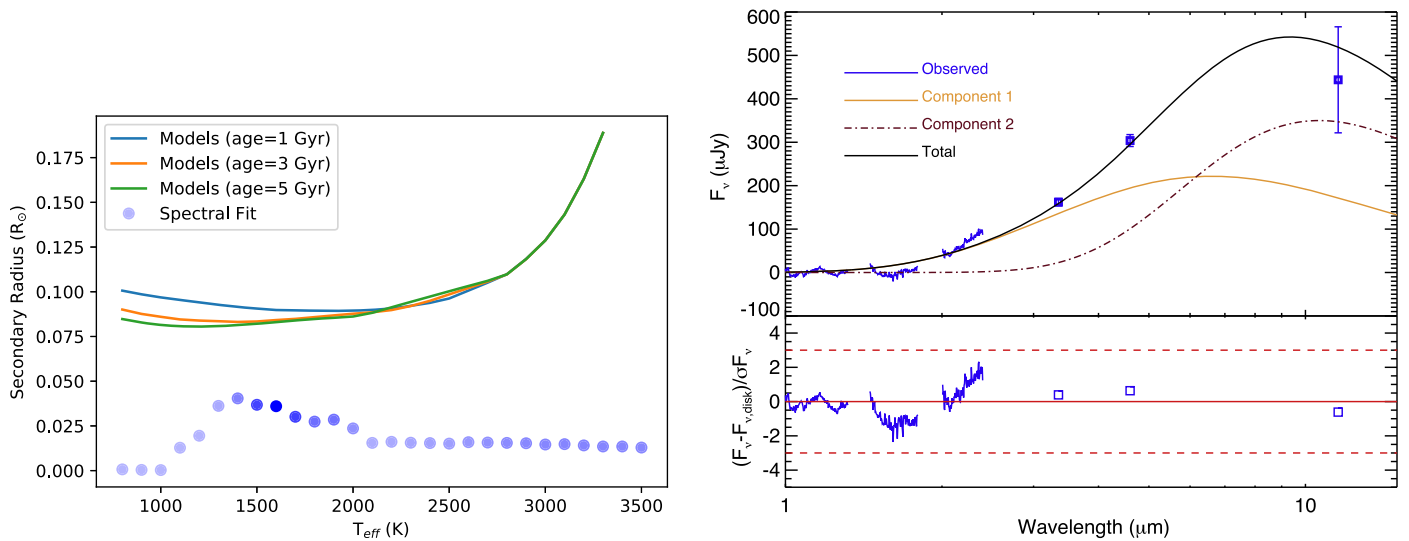


Figure 4. Left panel: we investigated the possibility that the IR excess was due to a cool companion by comparing different BT Settl models to the data. The best-fit models implied anomalously small radii based on the NIRES spectrum. Right panel: we subtracted off the flux from the best-fit white dwarf model to construct an SED of the residual IR excess around LSPM J0207+3331. Blue points are the rebinned NIRES spectrum and *WISE* photometry. We show a plausible model for the excess: a two-component disk that includes an optically thick inner region (Component 1; orange solid curve) and an optically thin structure near the edge of the white dwarf tidal disruption radius (Component 2; purple dashed–dotted curve). Component 1 has an inner disk temperature of 1400 K, and an outer temperature of 550 K. Component 2 is assumed to be an optically thin 480 K blackbody with an effective area of 10^{21} cm^2 . The lower panel shows the residuals against our disk model for the NIRES spectra and the *WISE* photometry, with the red dashed lines denoting $\pm 3\sigma$ residuals.

for lower density material such as ice or porous rubble, did not solve the poor fit to the data.

As an alternative approach to explain the observed SED, we posit a hybrid combination of an optically thick face-on disk and a single temperature blackbody as a plausible fit to the observed photometry. For the interior optically thick disk, we assume an inner temperature of 1400 K and outer temperature of 550 K, corresponding to an inner and outer radius of $0.047 R_{\odot}$ and $0.21 R_{\odot}$, respectively. We next assume a second component corresponding to a cooler optically thin dust distribution with a bulk temperature of 480 K. To fit the observed dust SED requires an effective surface area of 10^{21} cm^2 . The two components thus have a combined $L_{\text{IR}}/L_{\star} = 0.14$. The proposed model is compared to the observations in Figure 4, assuming that the NIRES spectra have a systematic 5% uncertainty on the relative flux calibration. This model simultaneously fits the short wavelength emission as well as the longer wavelength emission. While background contamination in the mid-IR is possible, the common proper motion of the *WISE* W1 and W2 sources with LSPM J0207+3331 suggests that contamination is unlikely. Mid-IR spectroscopy of this object with the *James Webb Space Telescope* should better constrain the structure and composition of the disk, as well as test whether or not there is a need for multiple components to the disk as implied by the W2 and W3 photometry.

Another possible explanation for the large W2 and W3 fluxes that does not require cold dust remains. For highly magnetic white dwarfs, the accretion of material onto the white dwarf surface also results in IR emission from cyclotron radiation (Debes et al. 2012; Parsons et al. 2013). However, the W2 single-epoch photometry rms over 94 epochs between 2014–2017 is 0.19 mag, while the median reported uncertainty on the photometry is 0.18 mag. One might expect large W2 variations for cyclotron radiation, so without further information we rate this alternative as unlikely.

Given the adopted temperature and effective surface area under the assumption of optically thin blackbody emission from a narrow ring of grains, we can speculate about the location and mass of the dust present. Assuming blackbody absorbing grains, we calculate that an optically thin distribution of dust will have an equilibrium temperature of 480 K at $\sim 0.94 R_{\odot}$, conveniently near the Roche radius of the white dwarf assuming a bulk density of water ice, or just outside it if the dust is composed of refractory material with higher density. The presence of this component over the ~ 7 yr of the *WISE* mission means that Poynting–Robertson (PR) drag has not had time to remove grains, thereby limiting the minimum grain radius of the dust distribution to $s \sim 8 \mu\text{m}$ for the mass and luminosity of LSPM J0207+3331 (Gustafson 1994). If the dust is $\sim 8 \mu\text{m}$ in radius, the total surface area (A) inferred by our blackbody fits implies a total minimum mass of $A/(\pi s^2) m_{\text{grain}} = 3.4 \times 10^{17} g (\rho/1 \text{ g cm}^{-3})$, which is equivalent to a small asteroid or comet.

4. Discussion

The discovery of LSPM J0207+3331 as a cool white dwarf with a significant IR excess makes new demands of models that seek to explain dust around white dwarfs. The first demand is that this discovery pushes the latest observable IR excess to ~ 3 Gyr after white dwarf formation, a factor of three larger than previous discoveries indicated. Current models for delivering planetesimals inside the tidal disruption radius of a white dwarf struggle to deliver the requisite mass of material to create an observable IR excess beyond the first Gyr of a white dwarf’s lifetime, especially if the white dwarf is not part of a binary (Bonsor & Wyatt 2010; Debes et al. 2012; Frewen & Hansen 2014; Veras et al. 2014a, 2014b, 2015, 2017; Mustill et al. 2018; Smallwood et al. 2018).

Second, dynamical models must now reproduce the observed frequency of detectable disks as a function of cooling age out to 3 Gyr. We have queried the *Gaia* DR2 catalog along with

AllWISE cross-matches for white dwarfs with similar $G - G_{RP}$ colors and distances < 200 pc (implying a range of T_{eff} between 5000 and 7000 K) with $W1$ and $W2$ detections to estimate the possible frequency of disks similar to LSPM J0207+3331. The full ADQL constraints we used were

$$\text{gaia.parallax} > 5 \quad (1)$$

$$\text{AND parallax/parallax_error} > 20 \quad (2)$$

$$\text{AND } G_{\text{abs}} > 5(G - G_{RP}) + 10 \quad (3)$$

$$\text{AND } G_{\text{abs}} < 16.3 \quad (4)$$

$$\text{AND } G_{\text{abs}} > 9.5 \quad (5)$$

$$\text{AND } G - G_{RP} > 0.33 \quad (6)$$

$$\text{AND } G - G_{RP} < 0.62 \quad (7)$$

$$\text{AND } W1 < 16. \quad (8)$$

We note that we do not apply many of the quality filters suggested to select white dwarfs by Gentile Fusillo et al. (2019), instead relying on high-significance parallaxes $\pi/\sigma\pi > 20$. Out of 346 candidate white dwarfs, only 5 had $W1-W2 > 0.3$ including LSPM J0207+3331. The candidates are: LSPM J1345+0504 (two faint galaxies within $5''$), 2MASS J21403597+7739195 (WD+M), 2MASS J18333593+5812176 (WD+M), and WISEA J032245.51+390445.0 (WD+M). This preliminary census implies a dust disk frequency of $\sim 0.2\%$, nearly an order of magnitude smaller than the frequency of dust disks around younger WDs.

Third, the IR excess seen for this disk requires a second, colder ring of dusty material that could potentially signal the presence of a gap in the system, or a component of dust that extends beyond the outer edge of the inner disk. If the second ring is confirmed, it would be the first example of a two-component ring system around a dusty white dwarf. If the dust disk has a gap near $0.94 R_{\odot}$, this implies the possibility of a body that continuously clears dust from the system, as the PR drag timescale is so short.







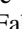


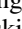
Finally, the presence of an optically thick disk at late white dwarf cooling times affords an interesting test of dust disk accretion. The accretion rate from optically thick disks is likely mediated by PR drag and is thus dependent on the luminosity and temperature of the white dwarf (Rafikov 2011). Models of disk accretion predict a slowly decreasing minimum accretion rate for a detectable disk, and older white dwarfs appear less likely to accrete at a high enough rate to yield an observable disk (Hollands et al. 2018). Based on the predictions of this model, LSPM J0207+3331 should have an accretion rate larger than $\sim 3 \times 10^7 \text{ g s}^{-1}$, a prediction that can be tested by taking an optical spectrum of this white dwarf to look for metal lines from accreted dust.

We would like to thank the many Zooniverse volunteers who have participated in the Backyard Worlds: Planet 9 project. We would also like to thank the Zooniverse web development team for their work creating and maintaining the Zooniverse platform and the Project Builder tools. Additionally, we thank the anonymous referee for suggestions that improved the manuscript. This research was supported by NASA ADAP grant NNH17AE75I. Some of the data presented herein were obtained at the W. M. Keck Observatory, which is operated as a scientific partnership among the California Institute of Technology, the University of California and the National Aeronautics and Space Administration. The Observatory was made possible by the generous financial support of the W. M.

Keck Foundation. The authors wish to recognize and acknowledge the very significant cultural role and reverence that the summit of Maunakea has always had within the indigenous Hawaiian community. We are most fortunate to have the opportunity to conduct observations from this mountain. This research has made use of the VizieR catalog access tool, CDS, Strasbourg, France. The original description of the VizieR service was published in A&AS 143, 23. This research has also made use of “Aladin sky atlas” developed at CDS, Strasbourg Observatory, France. DA spectroscopic models used in this Letter were obtained from the Spanish Virtual Observatory Theoretical Model Services site.

Facilities: Keck:II (NIRES), WISE.

ORCID iDs

John H. Debes  <https://orcid.org/0000-0002-1783-8817>
 Marc J. Kuchner  <https://orcid.org/0000-0002-2387-5489>
 Adam J. Burgasser  <https://orcid.org/0000-0002-6523-9536>
 Adam C. Schneider  <https://orcid.org/0000-0002-6294-5937>
 Aaron M. Meisner  <https://orcid.org/0000-0002-1125-7384>
 Jonathan Gagné  <https://orcid.org/0000-0002-2592-9612>
 Jacqueline K. Faherty  <https://orcid.org/0000-0001-6251-0573>
 Michael Cushing  <https://orcid.org/0000-0001-7780-3352>
 John Wisniewski  <https://orcid.org/0000-0001-9209-1808>
 Katelyn Allers  <https://orcid.org/0000-0003-0580-7244>

References

- Allard, F., Homeier, D., & Freytag, B. 2012, *RSPTA*, 370, 2765
 Baraffe, I., Chabrier, G., Barman, T. S., et al. 2003, *A&A*, 402, 701
 Barber, S. D., Kilic, M., Brown, W. R., et al. 2014, *ApJ*, 786, 77
 Bergeron, P., Wesemael, F., Dufour, P., et al. 2011, *ApJ*, 737, 28
 Bianchi, L., Conti, A., & Shiao, B. 2014, *AdSpR*, 53, 900
 Bonsor, A., Farihi, J., Wyatt, M. C., et al. 2017, *MNRAS*, 468, 154
 Bonsor, A., & Wyatt, M. 2010, *MNRAS*, 409, 1631
 Burrows, A., Hubbard, W. B., Lunine, J. I., et al. 2001, *RvMP*, 73, 719
 Caselden, D., Westin, P., III, Meisner, A., Kuchner, M., & Colin, G. 2018, *WiseView: Visualizing motion and variability of faint WISE sources*, Astrophysics Source Code Library, ascl:1806.004
 Chambers, K. C., Magnier, E. A., Metcalfe, N., et al. 2016, arXiv:1612.05560
 Cushing, M. C., Vacca, W. D., & Rayner, J. T. 2004, *PASP*, 116, 362
 Debes, J. H., Hoard, D. W., Farihi, J., et al. 2012, *ApJ*, 759, 37
 Debes, J. H., Hoard, D. W., Wachter, S., et al. 2011, *ApJS*, 197, 38
 Debes, J. H., & Sigurdsson, S. 2002, *ApJ*, 572, 556
 Debes, J. H., Walsh, K. J., & Stark, C. 2012, *ApJ*, 747, 148
 Denny, E., Clemens, J. C., Debes, J. H., et al. 2017, *ApJ*, 849, 77
 Farihi, J., Zuckerman, B., & Becklin, E. E. 2008, *ApJ*, 674, 431
 Frewen, S. F. N., & Hansen, B. M. S. 2014, *MNRAS*, 439, 2442
 Gaia Collaboration, Brown, A. G. A., Vallenari, A., et al. 2018, *A&A*, 616, A1
 Gentile Fusillo, N. P., Tremblay, P.-E., Gänsicke, B. T., et al. 2019, *MNRAS*, 482, 4570
 Gustafson, B. A. S. 1994, *AREPS*, 22, 553
 Hoard, D. W., Debes, J. H., Wachter, S., et al. 2013, *ApJ*, 770, 21
 Holberg, J. B., & Bergeron, P. 2006, *AJ*, 132, 1221
 Hollands, M. A., Gänsicke, B. T., & Koester, D. 2018, *MNRAS*, 477, 93
 Jura, M. 2003, *ApJL*, 584, L91
 Jura, M. 2008, *AJ*, 135, 1785
 Koester, D. 2010, *MmSAI*, 81, 921
 Koester, D., Gänsicke, B. T., & Farihi, J. 2014, *A&A*, 566, A34
 Kowalski, P. M., & Saumon, D. 2006, *ApJL*, 651, L137
 Kuchner, M. J., Faherty, J. K., Schneider, A. C., et al. 2017, *ApJL*, 841, L19
 Lépine, S., & Shara, M. M. 2005, *AJ*, 129, 1483
 Mainzer, A., Bauer, J., Cutri, R. M., et al. 2014, *ApJ*, 792, 30
 Mainzer, A., Bauer, J., Grav, T., et al. 2011, *ApJ*, 731, 53
 Meisner, A. M., Lang, D., & Schlegel, D. J. 2018, *AJ*, 156, 69
 Mustill, A. J., Villaver, E., Veras, D., et al. 2018, *MNRAS*, 476, 3939
 Parsons, S. G., Marsh, T. R., Gänsicke, B. T., et al. 2013, *MNRAS*, 436, 241
 Rafikov, R. R. 2011, *ApJL*, 732, L3
 Rocchetto, M., Farihi, J., Gänsicke, B. T., et al. 2015, *MNRAS*, 449, 574

- Skrutskie, M. F., Cutri, R. M., Stiening, R., et al. 2006, [AJ](#), **131**, 1163
- Smallwood, J. L., Martin, R. G., Livio, M., et al. 2018, [MNRAS](#), **480**, 57
- Theissen, C. A., West, A. A., Shippee, G., et al. 2017, [AJ](#), **153**, 92
- Tremblay, P.-E., & Bergeron, P. 2009, [ApJ](#), **696**, 1755
- Tremblay, P.-E., Bergeron, P., & Gianninas, A. 2011, [ApJ](#), **730**, 128
- Vacca, W. D., Cushing, M. C., & Rayner, J. T. 2003, [PASP](#), **115**, 389
- Veras, D., Eggl, S., & Gänsicke, B. T. 2015, [MNRAS](#), **452**, 1945
- Veras, D., Georgakarakos, N., Dobbs-Dixon, I., et al. 2017, [MNRAS](#), **465**, 2053
- Veras, D., Jacobson, S. A., & Gänsicke, B. T. 2014a, [MNRAS](#), **445**, 2794
- Veras, D., Shannon, A., & Gänsicke, B. T. 2014b, [MNRAS](#), **445**, 4175
- von Hippel, T., Kuchner, M. J., Kilic, M., Mullally, F., & Reach, W. T. 2007, [ApJ](#), **662**, 544
- Wilson, J. C., Henderson, C. P., Herter, T. L., et al. 2004, [Proc. SPIE](#), **5492**, 1295
- Wright, E. L., Eisenhardt, P. R. M., Mainzer, A. K., et al. 2010, [AJ](#), **140**, 1868
- Zuckerman, B., Koester, D., Melis, C., et al. 2007, [ApJ](#), **671**, 872